PERGAMON

International Journal of Heat and Mass Transfer 42 (1999) 4165–4183

International Journal of HEAT and MASS TRANSFER

www.elsevier.com/locate/ijhmt

Heat transfer and chemical reactions in exhaust system of a cold-start engine

S.H. Chan*, D.L. Hoang

School of Mechanical and Production Engineering, Nanyang Technological University, Nanyang Avenue, Singapore 639798, Singapore

Received 4 September 1998; received in revised form 12 February 1999

Abstract

Modelling of cold-start engine exhaust behaviour is a difficult task as it involves complicated heat transfer processes and chemical reactions at both the exhaust manifold/pipe and catalytic converter. This paper presents a model that is capable of predicting the exhaust gas temperatures along the exhaust pipe and across the catalyst monolith, both spatially and temporally. The dew point temperature platform, due to water condensation and subsequent evaporation, at catalysts downstream immediately after engine cold-start is successfully predicted. The conversions of toxic carbon monoxide and unburned hydrocarbons to harmless carbon dioxide and water at the catalytic converter are also validated satisfactorily by the experimental data. © 1999 Elsevier Science Ltd. All rights reserved.

Keywords: Modelling; Engine cold-start; Heat transfer; Chemical reaction; Catalytic converter; Dew point temperature

1. Introduction

Noxious emissions, such as carbon monoxide (CO), unburned hydrocarbons (uHC) and oxides of nitrogen (NO_x) in the exhaust of gasoline powered engines are effectively controlled by the adoption of three-way catalytic converter (TWC) whereby they are oxidised or reduced to harmless carbon dioxide (CO_2), nitrogen (N_2) and water vapour (H_2O). Today, TWC has become a common feature for the fuel injection gasoline engines with closed loop lambda feedback control. However, the catalytic converter will not be able to function effectively until it reaches the light-off/operating temperature, though TWC used in motor vehicles nowadays are able to achieve the reductions of CO, uHC and NO_x by up to 95% when they are fully warmed up. TWCs have been progressively improved in their design, structure, material properties, and hence performance. Ceramic converters with high cell density to increase surface area [1] and light weight ceramic with thin wall for low heat capacity [2] have been introduced for rapid catalysts light-off. However, the light-off temperatures of the TWCs are still not much different from the range of 250–340°C as reported by Burch et al. [3]. Recent research has revealed that 60–80% of the uHC and CO are emitted from a motor vehicle equipped with TWC within the first few minutes following engine cold start [4,5]. This peculiarity offers scope for the reduction of overall engine emissions; in particular where short journeys are frequently encountered in urban road driving.

To reduce the time spent on experiments and to optimise the complete exhaust system for improved

Abbreviations: CO, carbon monoxide; EMS, engine management system; NDIR, non-dispersive infra-red; NO_x, oxides of nitrogen; TWC, three-way catalytic converter; uHC, unburned hydrocarbon.

* Corresponding author.

PII: S0017-9310(99)00064-2

Nomenclature

C	gas concentration by volume (%)
c_p	heat capacity of pipe material (J/kg/K)
c_{pg}	specific heat of gas at constant pressure (J/kg/K)
D_j	mass diffusivity for gas species j (m^2/s)
d	hydraulic diameter of monolith cell channel (m)
d_1	pipe inner diameter (m)
d_2	pipe outer diameter (m)
d_{bent}	pipe bent diameter (m)
f	frictional factor
g	gravitational acceleration (9.81 m/s^2)
h	heat transfer coefficient (W/m^2/K)
h_{D_j}	mass transfer coefficient of gas species j
k	thermal conductivity (W/m/K)
k_j	kinetic rate constant (mol K/m^2/s) (j = 1, 4)
K_j	adsorption equilibrium constant (j = 1, 4)
M	molecular weight of gas (kg/kmole)
$\dot{m}$	mass flow rate of gas (kg/s)
Nu	Nusselt number
NTU	number of transfer unit
Pr	Prandtl number
Q	heat transfer (kJ)
q	heat flux (w/m^2)
R	reaction rate (mol/m^2/s)
R	universal gas constant (8.314 kJ/kg/K)
Ra	Rayleigh number
Re	Reynolds number
S	geometric surface area per unit catalyst volume (1/m)
Sc	Schmidt number
S_{cat}	catalytic surface area per unit catalyst volume (1/m)
Sh	Sherwood number
T	temperature (K)
t	time (s)
u	axial gas velocity (m/s)
V_1	volume of gas (m^3)
V_2	volume of pipe segment (m^3)
x	axial coordinate of exhaust system (m)
ΔF	surface area of monolith segment exposed to heat transfer (m^2)
ΔH	exothermal heat release (kJ/kmol)

Greek letters

α	thermal diffusivity (m^2/s)
β	volumetric thermal expansion coefficient (1/K)
μ	dynamic viscosity (kg/ms)
ν	kinematic viscosity (m^2/s)
ρ	density (kg/m^3)
σ	Stefan–Boltzmann constant (5.67×10^{-8} W/m^2 K^4)
δ	void fraction of the monolith
ε	surface roughness (m), emissivity

Subscripts

a	air
c	critical
cva	convection to ambient
g	gas
i	spacing grid
j	gas species j
gp	convection between exhaust gas and pipe wall
p	pipe
rad	radiation
s	catalyst surface

Superscripts

n	time step
in	inlet

catalyst lightoff, many modelling works have been conducted along with the experiments. Some simulation studies focused on predicting the thermal response of the exhaust gas in the air-gap dual-pipe exhaust system to improve exhaust pipe design for exhaust energy preservation [6,7], while others focused on predicting the conversion behaviours of the catalytic converters and their design optimisation. Yaegashi et al. [8] applied the simulation technique to optimise the heating pattern of an electrically heated catalyst. Baba et al. [9] used a 2-D simulation model to investigate the effects of the loading quantity of the noble metals for improved catalyst conversion efficiency. Koltsakis et al. [10] developed a 2-D model for TWC to study the effects of operating conditions (gas flow pattern and catalyst ageing) on the catalyst performance. These models separately studied thermal responses of the gas in the exhaust pipe and the performance of the catalytic converter at steady state or transient conditions with given constant inlet gas parameters. However, none of the above-mentioned models consider the actual engine cold-start conditions where the wall temperatures of the exhaust system and the catalytic converter are gradually heated up by the exhaust gas. Furthermore, significant amount of water vapour condensed onto the surfaces (and later evaporated) of the

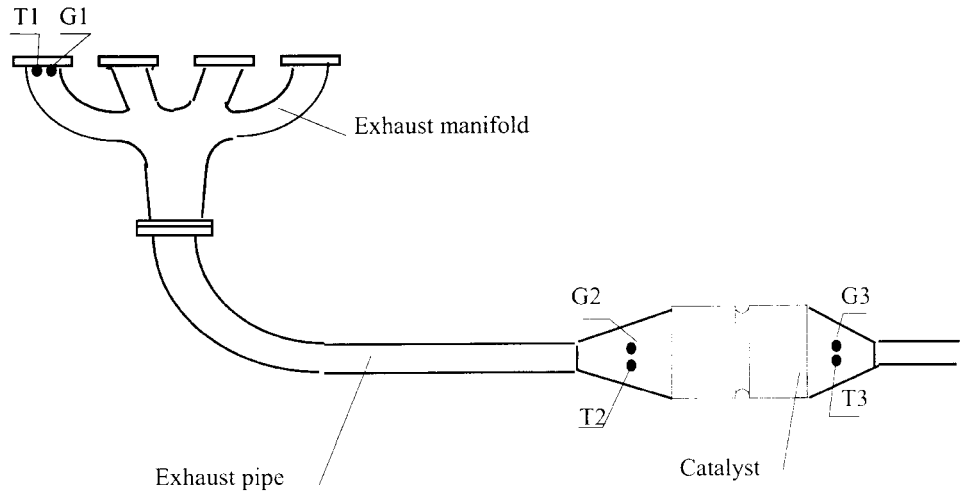

Fig. 1. Schematic layout of exhaust system (T and G: temperature and gases tapping points).

exhaust system and monolith cells during this engine cold-start phase and its effect on surface heat transfer were not considered thus far by any models.

The objective of this project is to develop a model, which considers detailed heat transfer processes and chemical reactions in the engine exhaust system, so that the performance of the catalytic converter and its light-off temperature can be accurately predicted. The predictive capability of the model is validated satisfactorily with the experimental data and is useful as a tool for matching of exhaust manifold/pipe and TWC and for improving catalyst light-off by means of exhaust system optimisation.

2. Exhaust system modelling

Simulation of the engine exhaust system equipped with a TWC is a useful and powerful tool not only for the engine designers to develop a new exhaust system, but also for researchers to find possible solutions for emissions control to meet the increasingly stringent emissions standards. Reliable and efficient simulations could reduce the number of experiments for engine system design and hence saving the cost. In addition, simulation technique allows one to study, in greater detail, the effects of some parameters that had been neglected or hardly to be achieved in the experiments. For example, when one simulates the effect of cold ambient air on the engine performance in a hot climate country, it is hardly and costly to be achieved by the experimental method.

Fig. 1 depicts the exhaust system of a 4-cylinder Ford engine equipped with a TWC under investigation. The exhaust system consists of three distinct parts, which include an exhaust manifold, an exhaust pipe and a catalytic converter.

2.1. Heat transfer in exhaust pipe

Fig. 2 shows schematically the pipe flow and its associated heat transfer elements that are represented by a control volume. Since the actual flow in the exhaust pipe is unsteady and compressible, the flow condition at any location of interest is described by three independent variables, i.e. velocity, density and pressure. However, as the emphasis of the current study is placed on the thermal effect on the exhaust system, the effect of the flow pulsation due to pressure wave actions on heat transfer process is simplified by adopting a pulsation factor in the Nusselt equation. By assuming a quasi-steady, incompressible flow, the 1-D energy equations for the exhaust gas and pipe wall take the form as below:

$$\frac{\partial T_g}{\partial t} + u\frac{\partial T_g}{\partial x} = -\frac{q_{gp}}{\rho_g c_{pg} V_1} \tag{1}$$

$$\frac{\partial T_p}{\partial t} = \alpha\frac{\partial^2 T_p}{\partial x^2} + \frac{q_{gp} - q_{cva} - q_{rad}}{\rho_p c_p V_2}. \tag{2}$$

Eq. (2) is actually a 1-D, unsteady, heat conduction equation with uniform thermal conductivity applied to the pipe wall.

2.1.1. Heat convection from exhaust gas to pipe wall

The heat transfer from the exhaust gas to the inner

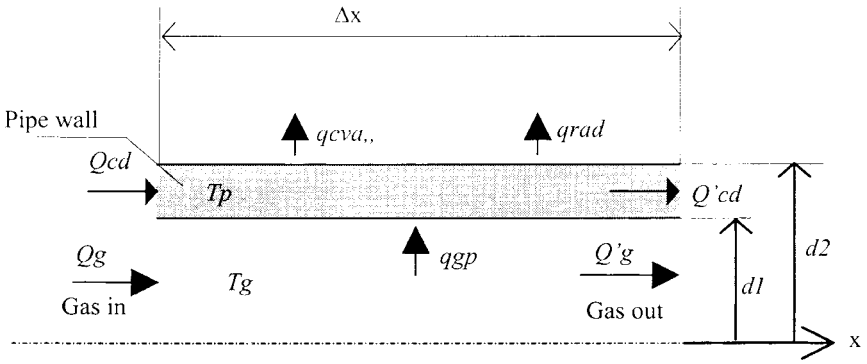

Fig. 2. Control volume of an exhaust pipe.

wall of the exhaust pipe is mainly due to the forced convection and is strongly dependent on the exhaust flow characteristics and the geometry of the pipe. The heat flux is expressed as:

$$q_{gp} = h_{gp}\pi d_1 \Delta x(T_g - T_p) \tag{3}$$

where h_{gp} is the convective heat transfer coefficient between the exhaust gas and the pipe wall, and is determined by the following Nusselt number:

$$Nu = \frac{h_{gp}d_1}{k_g}. \tag{4}$$

At engine cold-start, the cold pipe walls quench the hot exhaust gases from the engine, thus forming a thin layer of water film on the pipe wall affecting the heat transfer processes. Two cases were considered in this study, i.e. wet wall and dry wall heat transfers.

2.1.1.1. Wet surface heat transfer. When an engine is started from cold, the water vapour present in the hot exhaust gas is condensed onto the cold surfaces of the exhaust pipe forming a thin layer of water film, which is subsequently evaporated when the exhaust pipe temperature is in thermal equilibrium with the exhaust gas. The condensation and evaporation occur simultaneously and the process ceases when the pipe wall temperature exceeds the dew point temperature of water vapour. In the case that the pipe wall temperature is below the saturated temperature of the water vapour at a typical vapour pressure, condensation will dominate over the evaporation and vice versa. The wet surface serves as the media for heat transfer from the exhaust gas to the pipe wall. Heat transfer phenomena during the engine cold-start period is very complicated as it involves liquid and vapour phases and is beyond the scope of present study. Instead, an empirical correlation for wet surface heat transfer is adopted to account for the effect of water film on the heat transfer. A commonly used Dittus–Boelter correlation [11,12] for wet surface heat transfer is adopted

$$Nu = \frac{h_{gp}\, d_1}{k_g} = 0.023 Pr^{0.4} Re^{0.8} \tag{5}$$

where

$$Re = \frac{Gd_1}{\mu} \tag{6}$$

$$Pr = \frac{c_p \mu}{k_g} \tag{7}$$

$$G = \frac{4\dot{m}}{\pi d_1^2}. \tag{8}$$

The thermal properties of the gas are evaluated at $(T_g + T_{sat})/2$.

2.1.1.2. Dry surface heat transfer (fully warmed up exhaust pipe). When the exhaust pipe is fully warmed up, the Nusselt correlation for a fully developed flow based on the average flow rate of the exhaust gas is used. There are a number of heat transfer correlations available. Among all, a widely used correlation proposed by Gnielinski [13] was chosen for the present study.

For $10^4 < Re < 5 \times 10^6$

$$Nu = \frac{(f/8)(Re)Pr}{1.07 + 12.7(f/8)^{1/2}(Pr^{2/3} - 1)} \tag{9}$$

for $Re < 10^4$

$$Nu = \frac{(f/8)(Re - 1000)Pr}{1.07 + 12.7(f/8)^{1/2}(Pr^{2/3} - 1)} \tag{10}$$

where the friction factor (f) is determined by the fol-

lowing equation:

$$\frac{1}{\sqrt{f}} + 2\ \log\left(\frac{\varepsilon}{3.7d} + \frac{2.51}{Re\sqrt{f}}\right) = 0. \tag{11}$$

The thermal properties of gas are evaluated at T_g.

To take into account the effect of pipe bend on the heat transfer coefficient, Hausen [14] recommended the following correlation for the bend factor:

$$F_B = \frac{Nu_{bent-pipe}}{Nu} = 1 + \frac{21d_1}{Re^{0.14}d_{bent}}. \tag{12}$$

In addition, a gas pulsation factor (F_{pul}) with values between 1.6–3 [6,15] is introduced to the Nusselt correlation to account for its effect on heat transfer process. Hence, Eqs. (9) and (10) become:

For $10^4 < Re < 5 \times 10^6$

$$Nu = \frac{(F_B)(F_{pul})(f/8)RePr}{1.07 + 12.7(f/8)^{1/2}(Pr^{2/3} - 1)}. \tag{13}$$

For $Re < 10^4$

$$Nu = \frac{(F_B)(F_{pul})(f/8)(Re - 1000)Pr}{1.07 + 12.7(f/8)^{1/2}(Pr^{2/3} - 1)}. \tag{14}$$

2.1.1. Heat convection from pipe surface to ambient air

The heat flux from the outer surface of the pipe to the ambient air (q_{cva}) due to free heat convection is:

$$q_{cva} = h_{cva}\pi d_2 \Delta x(T_p - T_a) \tag{15}$$

where

$$h_{cva} = \frac{Nuk_a}{d_2}. \tag{16}$$

The Nusselt number is determined from the correlation proposed by Churchill and Chu [16] as below:

$$Nu = 0.6 + \left(\frac{0.387Ra^{1/6}}{[1 + (0.599/Pr)^{9/16}]^{8/27}}\right) \tag{17}$$

where

$$Ra = \frac{l^3 g\beta(T_p - T_a)}{\nu_a^2}Pr \tag{18}$$

and

$$\text{the wetted length } l = \pi d_2. \tag{19}$$

The property β is evaluated at T_a while other properties are evaluated at the film temperature T_f [17] below:

$$T_f = T_p - 0.38(T_p - T_a). \tag{20}$$

2.1.3. Heat radiation from pipe surface to surroundings

The radiative heat transfer rate from the pipe surface to surroundings is expressed by the following equation:

$$q_{rad} = \varepsilon\sigma\pi d_2(T_p^4 - T_a^4)\Delta x. \tag{21}$$

2.2. Heat and mass transfers in catalytic converter

Heat and mass transfers and chemical reactions are occurred simultaneously in the catalytic converter. The whole process is quite different between a fully warmed up catalytic converter and a warming up catalytic converter at engine cold start. In the early stage of the latter, condensation of water vapour present in the hot exhaust gas onto the surface of the monolith cells occurs. When the temperature of the monolith cells exceeds the dew point temperature of the water vapour, evaporation dominates and the process ceases when the monoliths cells are in thermal equilibrium with the exhaust gas. The phenomenon is quite similar to that occurred in the exhaust pipe, except that the surface exposed to water condensation and evaporation is much larger in the catalysts monolith. When monolith temperature reaches a range of 250–340°C, the chemical reactions occur and the converter is known to be activated [3]. The reactions take place at a very thin boundary layer in the neighbourhood of a gas/solid interface. At the vicinity of this boundary layer, the concentrations of main gas species are smaller than those in the mainstream through the cell channels (due to the chemical reaction) causing a mass transfer, which is characterised by a mass transfer coefficient h_{D_i}.

Therefore, the phenomena in the catalytic converter are very complicated which involve chemical reactions, convection heat transfer between the solid matrix and exhaust gas, heat storage and conduction in the monolith and radiation heat transfer from the catalytic converter to the surroundings. Heat transfer by radiation can be significant only at high temperature and high temperature gradient of the monolith [18]. Hence, if the monolith converter's temperature falls within the range of 300–1000 K, the effect of heat radiation is negligible compared to the heat conduction, and varies between 0.02 and 0.66% in magnitude [19].

2.2.1. Chemical reactions

Chemical reactions in the monolith converter are very complicated. Typically, hundreds of reactions occur inside a converter, depending on the exhaust gas composition, the temperature and the washcoat com-

position of the catalyst [19]. In this context, only the reactions concerning the elimination of noxious emissions components are of interest. The oxidation of CO, uHC (in the form of C_xH_y) and H_2 occurs when oxygen is available and in the presence of an oxidation catalyst. The chemical reactions take place in many complicated steps, but the overall reactions are as follows:

$$CO + \frac{1}{2}O_2 \rightarrow CO_2 \tag{22}$$

$$C_xH_y + \left(x + \frac{y}{4}\right)O_2 \rightarrow xCO_2 + \frac{y}{2}H_2O \tag{23}$$

$$H_2 + \frac{1}{2}O_2 \rightarrow H_2O. \tag{24}$$

The unburned hydrocarbons are normally expressed as a total hydrocarbons which include 86% of fast oxidising propylene (C_3H_6) and 14% of slow oxidising methane (CH_4) [20].

The reduction of NO is due to its reactions with reducing agents such as CO, H_2 and uHC. The mechanisms of the reactions are listed below [4,21]:

$$NO + CO \rightarrow \frac{1}{2}N_2 + CO_2 \tag{25}$$

$$NO + H_2 \rightarrow \frac{1}{2}N_2 + H_2O \tag{26}$$

$$NO + (C_xH_y) \rightarrow N_2 + H_2O + CO_2. \tag{27}$$

Which mechanism above is in dominating role depends on the concentration and chemical activity of the respective reducing agent attending the reaction and the conditions of the reactions. In the TWC, CO is considered to be the main species participating in NO reduction [9,10,22,23], thus Eq. (25) is the dominating mechanism in the NO reduction. Since CO serves as the reducing agent for NO, the latter has become the oxidising agent for the former.

Review of the existing catalytic converter models shown that the basis of catalytic converter models is kinetic reaction rate expressions. Most of the existing models rely on Langmuir–Hinshelwood type kinetic rate expressions presented by Voltz et al. [24] with modified kinetic constants and activation energies.

2.2.2. Kinetic reaction rate expressions

In the exclusion of NO modelling in the present study, the mechanisms associated with the oxidation processes are summarised as follows:

$$R_1: \quad CO + \frac{1}{2}O_2 \rightarrow CO_2 \tag{28}$$

$$R_2: \quad C_3H_6 + 4.5O_2 \rightarrow 3CO_2 + 3H_2O \tag{29}$$

$$R_3: \quad CH_4 + 2O_2 \rightarrow CO_2 + 2H_2O \tag{30}$$

$$R_4: \quad H_2 + \frac{1}{2}O_2 \rightarrow H_2O. \tag{31}$$

The kinetic rate expressions associated with the above mechanisms are adopted from Voltz et al. [24] and Oh and Cavendish [25] and are listed as follows:

$$R_1 = R_{CO} = k_1 C_{S,CO} C_{S,O_2}/G \tag{32}$$

$$R_2 = R_{C_3H_6} = k_2 C_{s,C_3H_6} C_{s,O_2}/G \tag{33}$$

$$R_3 = R_{CH_4} = k_3 C_{s,CH_4} C_{S,O_2}/G \tag{34}$$

$$R_4 = R_{H_2} = k_4 C_{s,H_2} C_{s,O_2}/G \tag{35}$$

where

$$G = T_S(1 + K_1 C_{S,CO} + K_2 C_{S,C_3H_6})^2(1 + K_3 C_{S,CO}^{2} C_{S,C_3H_6}^{2})(1 + K_4 C_{S,NO_x}^{0.7}). \tag{36}$$

The term $(1 + K_4 C_{s,NO_x}^{0.7}) = 1$ for not accounting for NO_x conversions and the adsorption equilibrium constants [24] are shown as follows:

$$K_1 = 65.5e^{\frac{961}{T_S}} \tag{37}$$

$$K_2 = 2.1 \times 10^3 e^{\frac{361}{T_S}} \tag{38}$$

$$K_3 = 4.0e^{\frac{11611}{T_S}} \tag{39}$$

$$K_4 = 4.8 \times 10^5 e^{\frac{-3773}{T_S}}. \tag{40}$$

The rate expression of the reaction of O_2 is calculated by balancing oxygen concentration in the above reactions [Eqs. (28)–(31)]. Thus,

$$R_5 = R_{O_2} = 0.5R_1 + 4.5R_2 + 2R_3 + 0.5R_4. \tag{41}$$

The kinetic rate constants in Eqs. (32)–(35) are as follows:

$$k_1 = 1.005 \times 10^{14} e^{\frac{-16\,574}{T_S}} \tag{42}$$

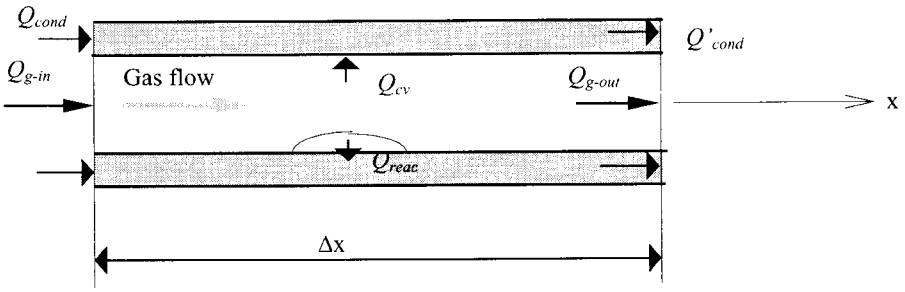

Fig. 3. Control volume of a monolith cell channel.

$$k_2 = 1.392 \times 10^{15} \mathrm{e}^{\frac{-19\,250}{T_s}} \tag{43}$$

$$k_3 = 7.32 \times 10^{10} \mathrm{e}^{\frac{-25\,080}{T_s}} \tag{44}$$

$$k_4 = k_1. \tag{45}$$

2.2.3. Catalytic converter mode

Fig. 3 depicts the monolith channel represented by a control volume with heat interactions. The assumptions made for the catalytic converter model are as below:

- Uniform properties at front face of the monolith.
- Heat radiation and conduction in the gas phase are negligible compared to the heat convection.
- Catalytic converter is well insulated (adiabatic).
- Gas temperatures and concentrations are identical for all cell channels.

Based upon the above assumptions, the basic equations for the catalytic converter model is nothing more than the mass and energy balances of the gas phase and solid phase of the converter.

For the gas phase, the mass and energy balances are:

$$\frac{\partial C_{gj}}{\partial t} = -u\frac{\partial C_{gj}}{\partial x} - h_{D_j} S(C_{gj} - C_{sj}) \tag{46}$$

$$\delta\rho_g c_{pg}\frac{\partial T_g}{\partial t} = -\rho_g u c_{pg}\frac{\partial T_g}{\partial x} + hS(T_s - T_g). \tag{47}$$

Since the time constant involved in the gas phase is much smaller than the thermal response of the solid phase the time derivative terms in the above equations can be neglected. Thus, Eqs. (46) and (47) become:

$$u\frac{\partial C_{gj}}{\partial x} = h_{D_j} S(C_{sj} - C_{gj}) \tag{48}$$

$$\rho_g u c_{pg}\frac{\partial T_g}{\partial x} = hS(T_s - T_g) \tag{49}$$

For the solid phase, the mass and energy balances are:

$$S_{Cat} R_j = \frac{\rho_g}{M} h_{D_j} S(C_{gj} - C_{sj}) \tag{50}$$

$$\begin{aligned}(1-\delta)\rho_s c_{ps}\frac{\partial T_s}{\partial t} &= (1-\delta)k_s\frac{\partial^2 T_s}{\partial x^2} + hS(T_g - T_s) \\ &+ S_{Cat}\sum_{j=1}^{5}(-\Delta H_j)R_j\end{aligned} \tag{51}$$

where subscript j denotes to gas component j ($j = 1$ for CO, 2 for C_3H_6, 3 for CH_4, 4 for H_2, 5 for O_2); C_j is concentration of gas j; $(-\Delta H)$ is the enthalpy of combustion and the prefixed '$-$' sign stands for the exothermic reaction. The value for enthalpy of combustion of each species is listed below [23,24,26]:

$$\Delta H_{CO} = -2.832 \times 10^5 \text{ kJ/kmol}$$

$$\Delta H_{C_3H_6} = -1.928 \times 10^6 \text{ kJ/kmol}$$

$$\Delta H_{CH_4} = -6.420 \times 10^5 \text{ kJ/kmol}$$

$$\Delta H_{H_2} = -2.420 \times 10^5 \text{ kJ/kmol.}$$

The boundary conditions for the catalyst monolith are as follows:

$$T_g(0,t) = T_g^{in} \tag{52}$$

$$C_{g,j}(0,t) = C_{g,j}^{in} \tag{53}$$

$$T_s(x,0) = T_a \tag{54}$$

$$\frac{dT_s}{dx}(0,t) = \frac{dT_s}{dx}(L,t) = 0. \quad (55)$$

2.2.4. Heat and mass transfer correlation

Similar to the phenomena occurred in the exhaust pipe, the heat transfers in the catalyst monolith include both wet surface and dry surface heat transfers. When the monolith's temperature is lower than that of the saturated temperature of the water vapour present in the exhaust gas, condensation of water vapour onto the cells wall occurred and wet surface heat transfer is dominated. In this process, the heat transfer correlation similar to Eq. (5) was applied. However, when the cells wall temperature exceeds the dew point temperature of the water vapour, evaporation of water film occurs and dry surface heat transfer is dominated. The heat transfer correlations are adopted from Baba et al. [9]:

$$h = \frac{Nuk_g}{d} \quad (56)$$

where

$$Nu = 0.571\left(Re\frac{d}{x}\right)^{2/3}. \quad (57)$$

The mass transfer coefficient (h_{D_j}) in Eqs. (48) and (50) is as follows:

$$h_{D_j} = \frac{ShD_j}{d} \quad (58)$$

$$Sh = 0.705\left(Re\frac{d}{x}\right)^{0.43} Sc^{0.56}. \quad (59)$$

The diffusivity of species j (D_j) used is a Slattery–Bird formula and is obtained from Bird [27]:

$$\frac{pD_j}{(p_{cj})^{2/3}(T_{cj})^{10/12}\left(\frac{2}{M}\right)^{1/2}} = a\left(\frac{T}{T_{cj}}\right)^b \quad (60)$$

where $a = 2.745 \times 10^{-4}$, $b = 2.334$.

3. Numerical solutions

3.1. Exhaust pipe

Numerical implementation for the exhaust pipe includes two successive steps. Firstly, wet surface heat transfer associated with the formation of thin layer of water film onto the inner surface of exhaust pipe until the wall temperature exceeds the saturation temperature of the water vapour in the exhaust gas. Secondly, dry surface heat transfer for the rest of the process. Eqs. (1) and (2) are solved simultaneously by finite-difference method. With the assumption of quasi-steady exhaust gas flow due to the time constants involved are typically much smaller than that of the solid thermal response, the time derivative term in Eq. (1) can be neglected. Eq. (1) is then solved by the number of transfer units (NTU) method. The whole length of the exhaust pipe is partitioned into discrete elements with grid space distance Δx. Thus, the gas temperature along the pipe at time step n with a time matching step Δt, becomes:

$$T_g|_{i+1}^n = T_p|_i^n + [T_g|_i^n - T_p|_i^n]e^{-NTU} \quad (61)$$

where

$$NTU = \frac{h_{gp}\pi d_1 \Delta x}{Mc_{pg}} \quad (62)$$

and subscripts i, n refer to the space and time marching indexes, respectively.

The NTU method has some advantages over the classical upwind method in terms of stability consideration [28]. The computation of the gas temperature during the space marching is not subject to any constraints in choosing the space step.

Eq. (2) is solved by forward-time, centred-space finite-difference approximation. Thus,

$$T_p|_i^{n+1} = T_p|_i^n + \alpha\frac{\Delta t}{\Delta x^2}(T_p|_{i+1}^n - 2T_p|_i^n + T_p|_{i-1}^n) + \left.\frac{\Delta t(q_{gp} - q_{cva} - q_{rad})}{\rho_p c_p(V_2 - V_1)}\right|_i^n \quad (63)$$

where the thermal state of the pipe at time step n had been calculated in the earlier step. The stability criteria according to Thomas [29] is as follow:

$$\alpha\frac{\Delta t}{\Delta x^2} \le \frac{1}{2}. \quad (64)$$

Based on the space domain of the exhaust system, the space grid (Δx) is chosen to be 2.5 mm and the corresponding time step-size (Δt), being 5 ms is estimated by satisfying the criteria above.

3.2. Catalytic converter

A system of 4 equations (Eqs. (48)–(51)) accompanied by 4 boundary conditions (Eqs. (52)–(55)) are solved simultaneously by finite-difference method in the catalytic converter model. Eqs. (48), (49) and (51) are non-linear partial differential equations while Eq. (50) is a non-linear algebraic equation relating the four unknowns T_g, T_s, C_{gi} and C_{si}. In the numerical

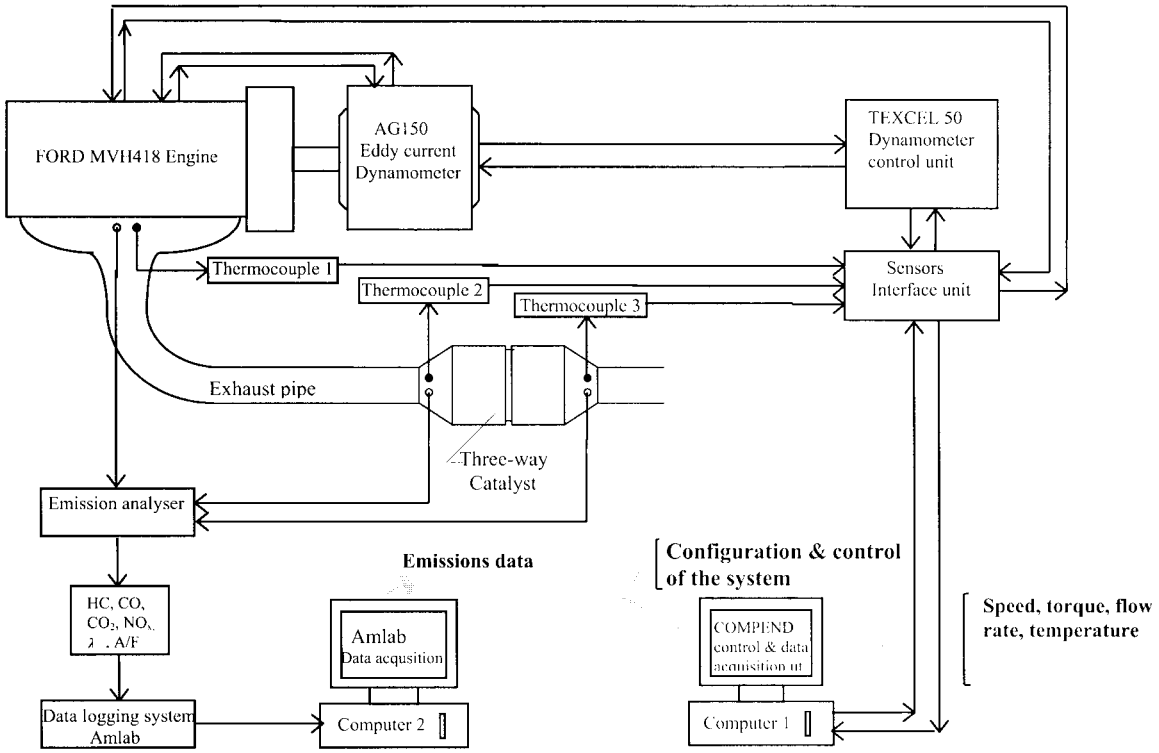

Fig. 4. Schematic arrangement of engine test bed facility.

treatment, the space grid (Δx) and time step-size (Δt) are chosen similar to those of the exhaust pipe. The heat and mass transfer processes within Δx during Δt were assumed to be steady. Therefore the transient behaviour of the catalytic converter was computed as a series of quasi-steady states. This approach is valid since the characteristic time constants involved in the transport and reaction phenomena are usually much smaller than the unsteady characteristic of the gas at the catalytic converter inlet.

With known boundary condition of Eq. (54), the solid temperature $T_s(x, t)$ is known in the first time step of iteration, then energy Eq. (49) together with boundary condition Eq. (52) was solved for T_g by employing locally analytical solutions based on the NTU method. Thus,

$$T_{g,i+1} = T_{s,i} + (T_{g,i} - T_{s,i})e^{-NTU_h} \tag{65}$$

where

$$NTU_h = \frac{h\Delta F}{\dot{m}_g c_{pg}}.$$

Eq. (48) is the mass balance equation for each exhaust gas species j. Integrating this equation over the monolith segment (Δx) of the catalytic converter gives the following correlation of gas concentration in the form of NTU. Thus,

$$C_{g,\,j+1} = C_{s,i} + (C_{g,i} - C_{s,i})e^{-NTU_m} \tag{66}$$

where

$$NTU_m = \frac{h_{D_j}\rho_g \Delta F}{\dot{m}_g}.$$

The local molar fluxes n_j for each species per unit catalyst volume are:

$$n_{j,i} = \frac{\dot{m}_g}{\Delta VM}(C_{g\,j,i} - C_{g\,j,i+1}). \tag{67}$$

Substituting Eq. (66) into Eq. (67) gives:

$$n_{j,i} = \frac{\dot{m}_g}{\Delta VM}(C_{g\,j,i} - C_{sj,i})(1 - e^{-NTU_m}). \tag{68}$$

Based upon the conservation of mass, the right-hand side of Eq. (68) must be equal to the right-hand side of Eq. (50). Therefore, the mass balance equation becomes:

$$S_{cat}R_j = \frac{\dot{m}_g}{\Delta VM}(C_{g\,j,i} - C_{sj,i})(1 - e^{-NTU_{mj}}). \tag{69}$$

The above equation is a non-linear algebraic equation, in which R_j is a function of $T_{s,i}$ and $C_{sj,i}$. Therefore, at

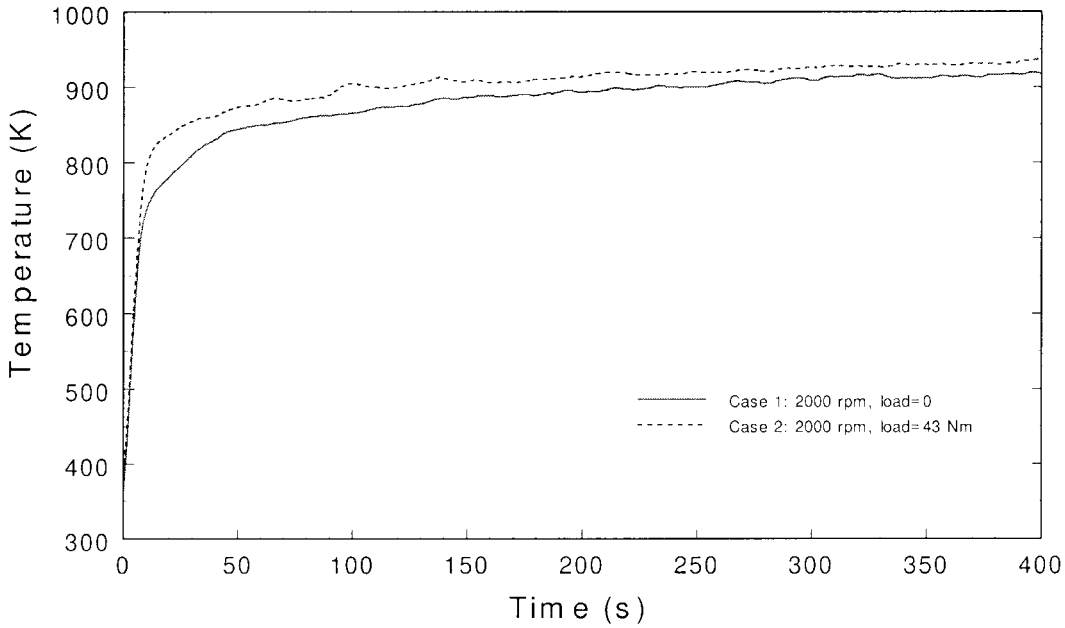

Fig. 5. Measured exhaust gas temperature at exhaust ports downstream.

time step t, with known boundary conditions Eqs. (53) and (54) for $C_{gj,i}$ and $T_{s,i}$, Eq. (69) contains only unknowns of C_{sj} (where $j = 1, 5$). This is a system of 5 simultaneous non-linear algebraic equations that can be solved for surface concentrations of CO, C_3H_6, CH_4, H_2 and O_2 by using the Newton's method [30]. Consequently, the gas concentration of each species is determined from Eq. (66) with boundary condition Eq. (53).

Finally, Eq. (51) associated with boundary conditions Eqs. (54) and (55) are solved for the catalytic converter temperature T_s using the forward-time centred-space finite-difference approximation [31] with stability criteria similar to that applied to the exhaust pipe.

3.3. Determination of water vapour concentration

The purpose of determination of water vapour concentration in the exhaust gas is to find its saturation temperature and hence deciding whether wet or dry surface heat transfer correlation should be applied for the walls of exhaust pipe and monolith cells.

Water concentration in the exhaust gas can be determined as follows. Firstly, water content in the intake air at ambient conditions was determined from psychrometric chart or by calculation based on the data from steam tables. For example, if the ambient conditions at the time of experiment are pressure of 1 atm, temperature of 30°C and relative humidity of 80%, the water content per kmol of dry air is 0.0351 kmol (water)/kmol (dry air). Secondly, the water vapour produced from fuel-air combustion was calculated based on chemical equilibrium of fuel–air reaction. Finally, the water concentration in the exhaust gas was determined, which is the sum of the two above-mentioned components. For a typical stoichiometric fuel–air reaction with similar ambient conditions, the water concentration in the exhaust gas is 16.6% by mole or 9.48% by mass. Hence, the partial pressure of water vapour (p_v) in the exhaust gas was determined. Thus

$$p_v = 0.166 p_g$$

where p_g is the exhaust gas pressure.

The dew point/saturated temperature of the water vapour at this partial water vapour pressure is then determined based on the steam tables or psychrometric chart (55–56°C in this case). When any surface temperature is lower than the dew point temperature of the gas, condensation occurs. Hence, determination of wet or dry surface heat transfer depends on whether the surface temperature of the exhaust pipe or the monolith cells is higher or lower than the calculated dew point temperature.

4. Experimental set up

Fig. 4 shows the schematic arrangement of the engine test bed. A fully instrumented Ford MVH 418 engine carried with a TWC is mounted on an eddy

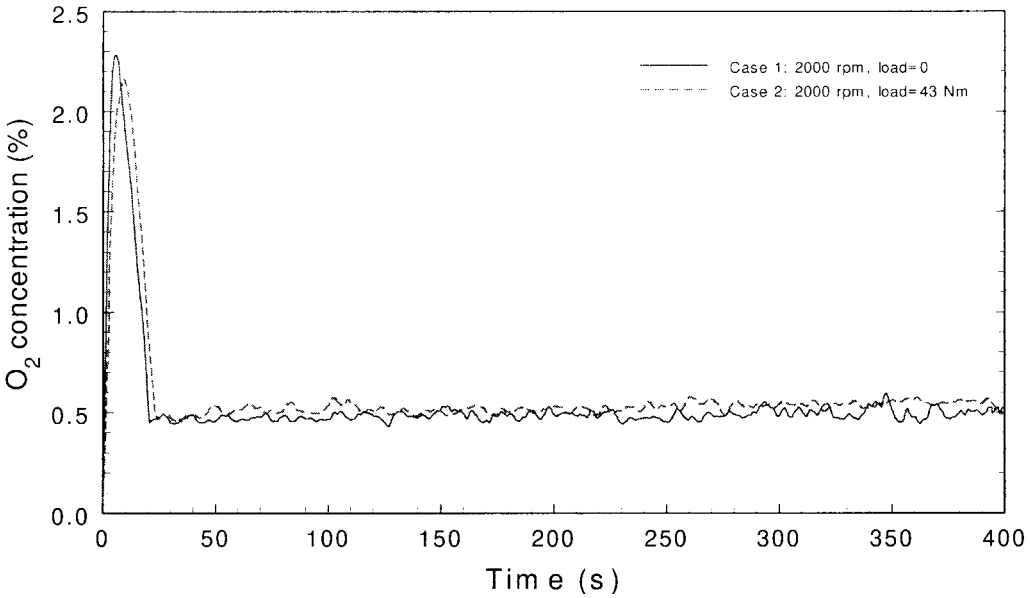

Fig. 6. Measured concentration at exhaust ports downstream.

current dynamometer. The engine is a 4-stroke, 4-cylinder, multi-point injection SI engine equipped with a fully electronic engine management system (EMS). The detailed specifications of the engine are given in Appendix A. The dynamometer has a maximum braking capacity of 150 kW at 8000 rpm and is controlled by a Texcel 50 controller complete with a remote control interface. The controller controls engine load, throttle and speed both manually and automatically. The latter is achieved by a computer where the test specifications can be configured by the users to perform a desired task. Apart from the engine supervisory role, the computer is also responsible for data acquisition, in particular performance

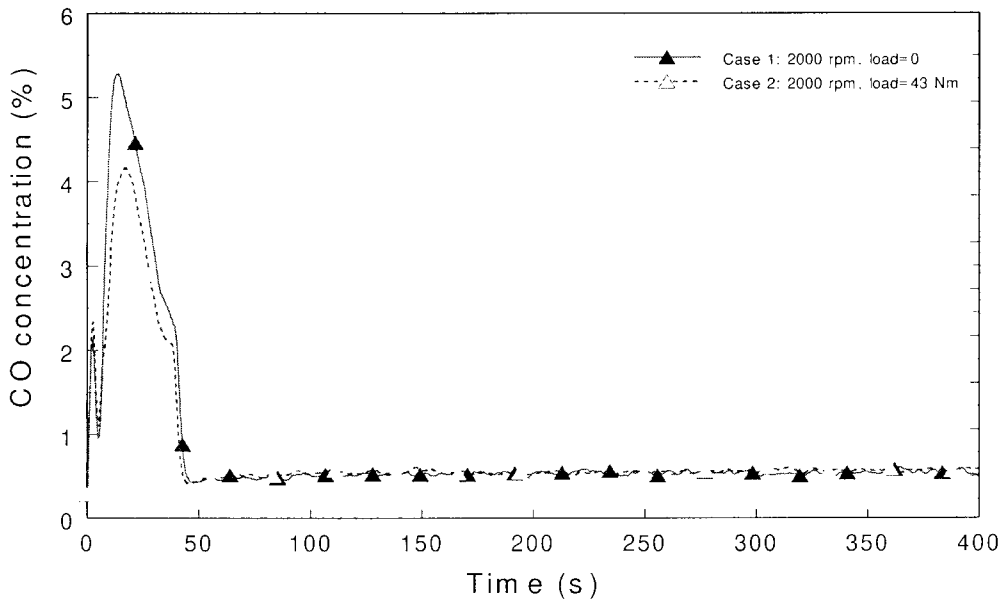

Fig. 7. Measured CO concentration at exhaust ports downstream.

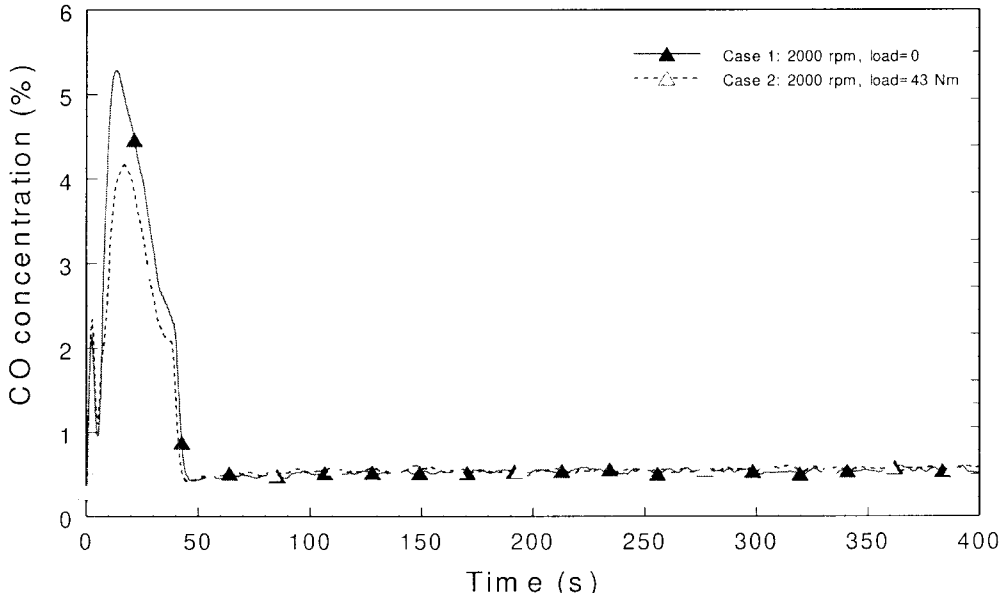

Fig. 8. Measured THC concentration at exhaust ports downstream.

related parameters and gas temperatures at various locations along the entire exhaust system. Emissions data, both CO and uHC were obtained from two multi-gas non-dispersive infrared (NDIR) analysers and were logged down by another computer configured to determine the conversion efficiency of the catalytic converter on-line.

The catalytic converter used is a two-piece TWC of 0.75 l, each with JM wash coat. The monolith is made of cordierite with 62 cpsc (400 cpsi) and loaded with catalysts of 2119 g/m^3. The converter is mounted on the exhaust system at 1.1 m away from the exhaust ports. The detailed specifications of the catalytic converter are given in Appendix B.

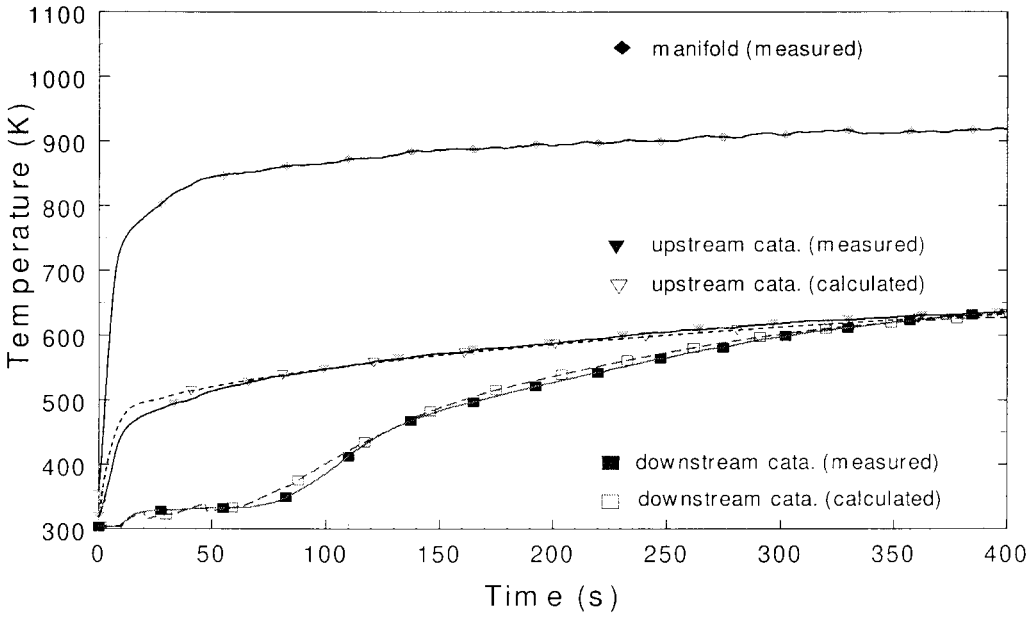

Fig. 9. Comparison of predicted exhaust gas temperatures with measured data at various tapping points (Case 1).

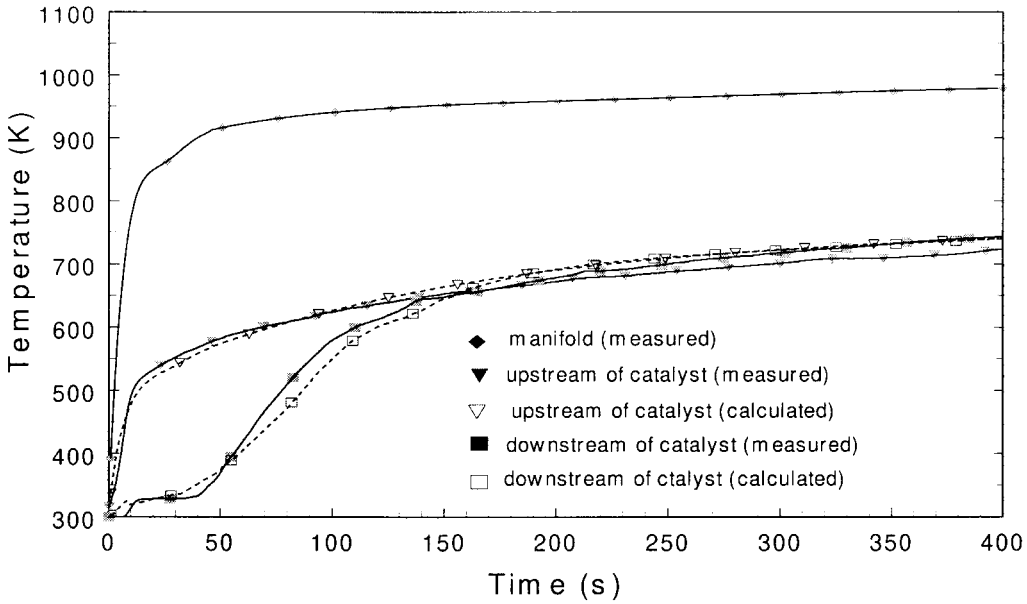

Fig. 10. Comparison of predicted exhaust gas temperatures with measured data at various tapping points (Case 2).

5. Results and discussions

Figs. 5–8 show the measured temperatures, concentrations of O_2, CO, THC, against the time respectively at the exhaust ports downstream for two cases of engine running conditions. Case 1 was set at no load with engine cranks to 2000 rpm immediately after engine firing, whilst Case 2 was set at 2000 rpm and 43 Nm. Significant variations of signals were seen in the first 50 s of engine running mainly due to the transient operations associated with engine warming up. Since the emphasis of current study is placed on the cold-start exhaust behaviour the engine was allowed to soak at ambient condition for at least 12 h or overnight to

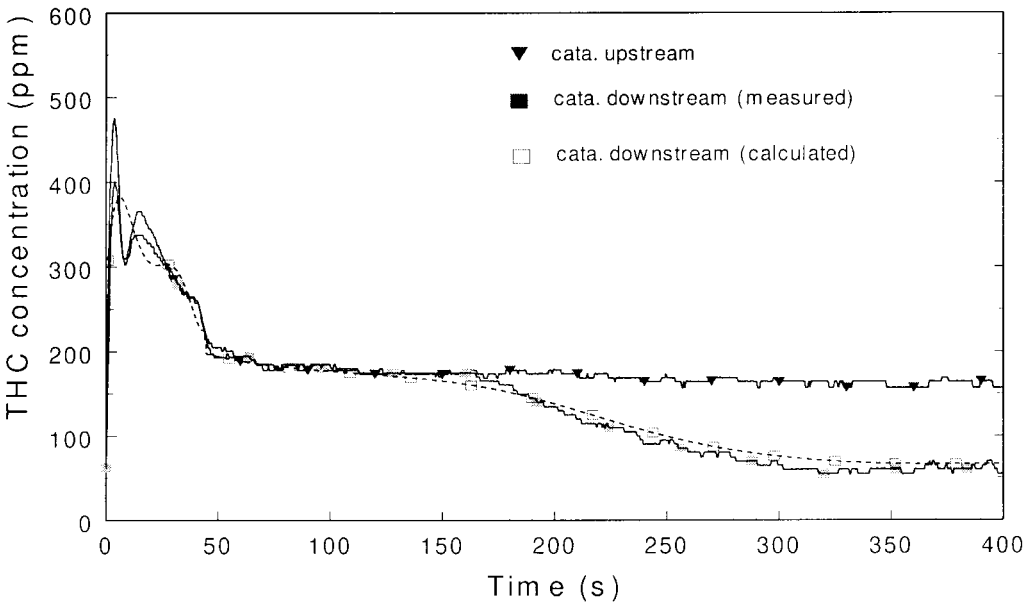

Fig. 11. Comparison of predicted THC concentrations at catalytic converter downstream with measured data (Case 1).

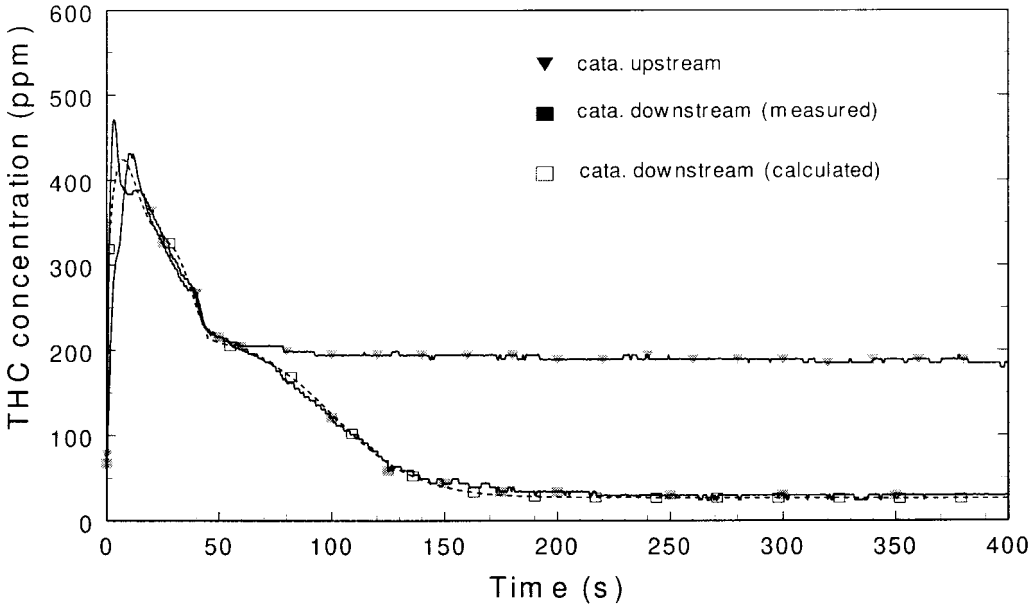

Fig. 12. Comparison of predicted THC concentrations at catalytic converter downstream with measured data (Case 2).

ensure that both engine and the catalyst were 'cold' before testing. The ambient pressure, temperature and relative humidity were measured at time the experiments were conducted. Fig. 6 shows that the oxygen concentration available for oxidising the CO and uHC varies from about 0.5–2.3%. Too lean the engine running conditions causing poor conversion efficiency of NO_x at the catalytic converter, though NO_x reduction was not included in this study.

Figs. 9 and 10 compare the predicted temperatures with measured data across the catalyst monolith for both Case 1 and Case 2 engine tests respectively. If

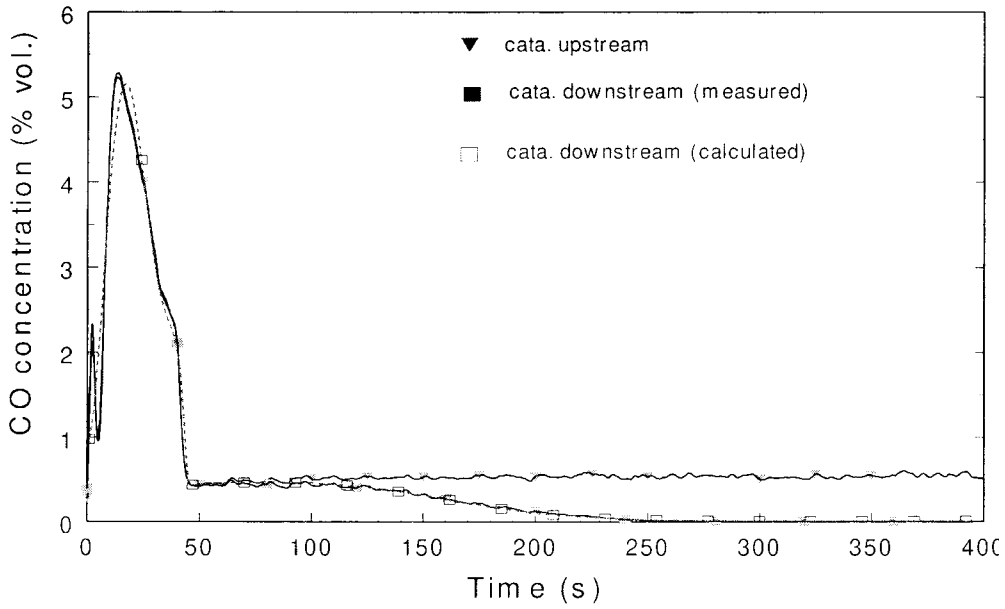

Fig. 13. Comparison of predicted CO concentrations at catalytic converter downstream with measured data (Case 1).

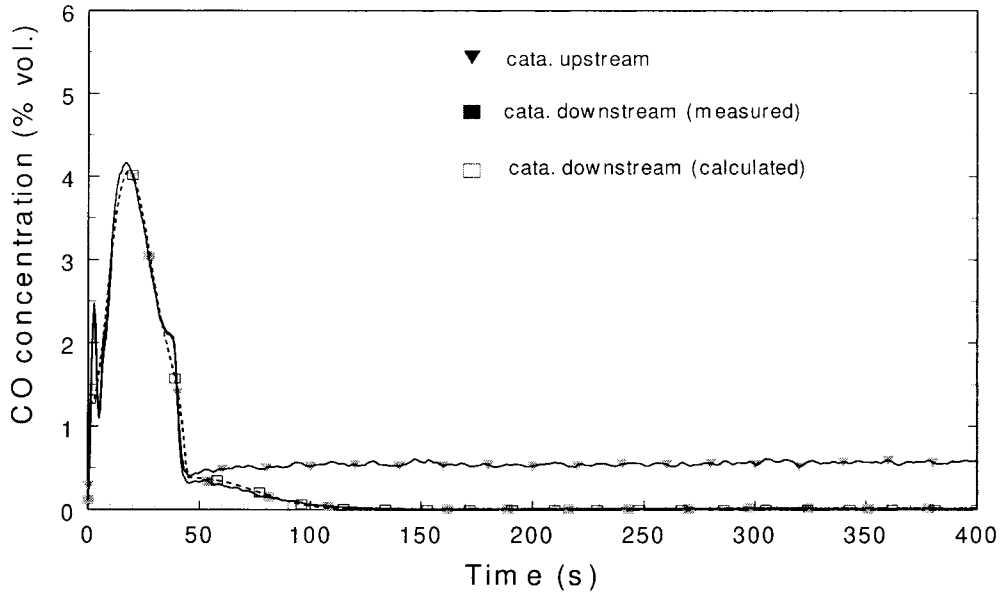

Fig. 14. Comparison of predicted CO concentrations at catalytic converter downstream with measured data (Case 2).

taking 573 K (300°C) as the activating point for catalysts lightoff, the times needed to achieve this (monolith upstream temperatures) are 150 s and 50 s for both Case 1 and Case 2, respectively. It is interesting to note that the dew point temperature platforms due to the water vapour condensation and subsequent evaporation occurred immediately after engine cold-start were satisfactorily predicted by the model. Intuitively, the lower exhaust temperature associated with no load operation in Case 1 would result in longer dew point temperature platform compared to Case 2.

Figs. 11 and 12 compare the predicted downstream THC concentrations with measured data for both

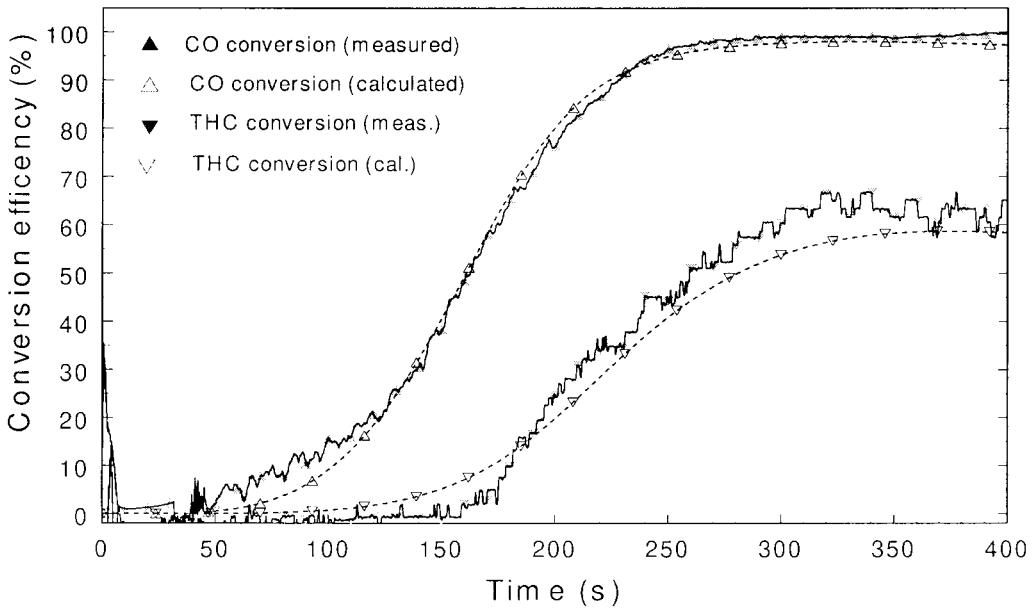

Fig. 15. Comparison of predicted conversion efficiencies of THC and CO with measured data (Case 1).

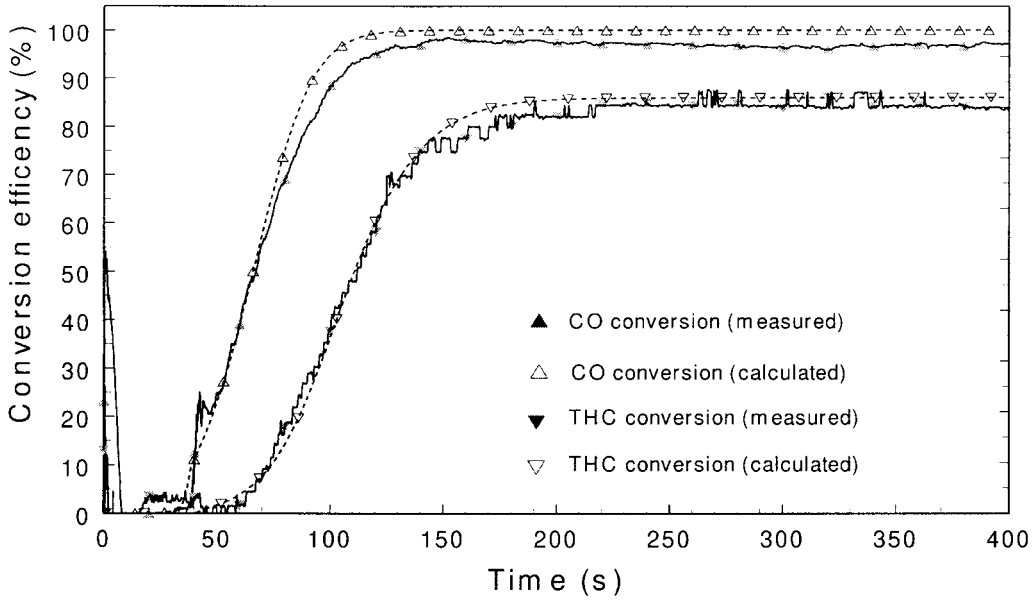

Fig. 16. Comparison of predicted conversion efficiencies of THC and CO with measured data (Case 2).

Case 1 and Case 2 engine tests respectively. The catalyst's activated point where the downstream THC departs from its upstream THC counterpart reflects the 300°C that is generally used as a guide for catalyst lightoff point. The predicted variations of the downstream THC against the time were validated satisfactorily and shown in both in Figs. 11 and 12. Figs. 13 and 14 show the predicted downstream CO concentrations with measured data for both Case 1 and Case 2 engine tests respectively. Both cases show that noticeable conversion of CO to CO_2 starts at around 50 s. Note that the post-flame oxidation in regions near to the exhaust ports were not considered and the emissions levels of CO and THC at the upstream catalyst monolith were taken as identical to those measured values at the exhaust ports downstream.

Figs. 15 and 16 compares the predicted conversion efficiencies of CO and THC with measured data for both Case 1 and Case 2 engine tests respectively. Fig.

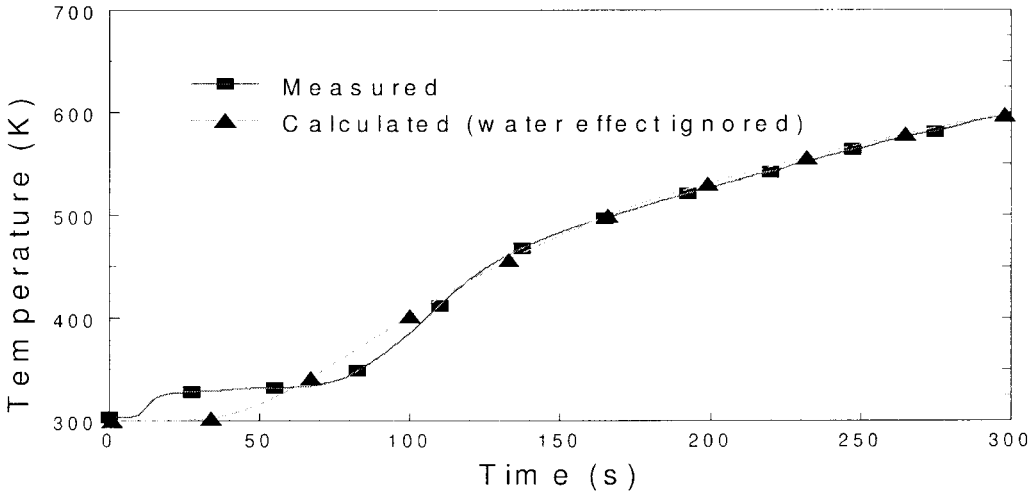

Fig. 17. Comparison of calculated gas temperature (with water condensation effect ignored) and measured gas temperature at catalyst downstream (Case 1).

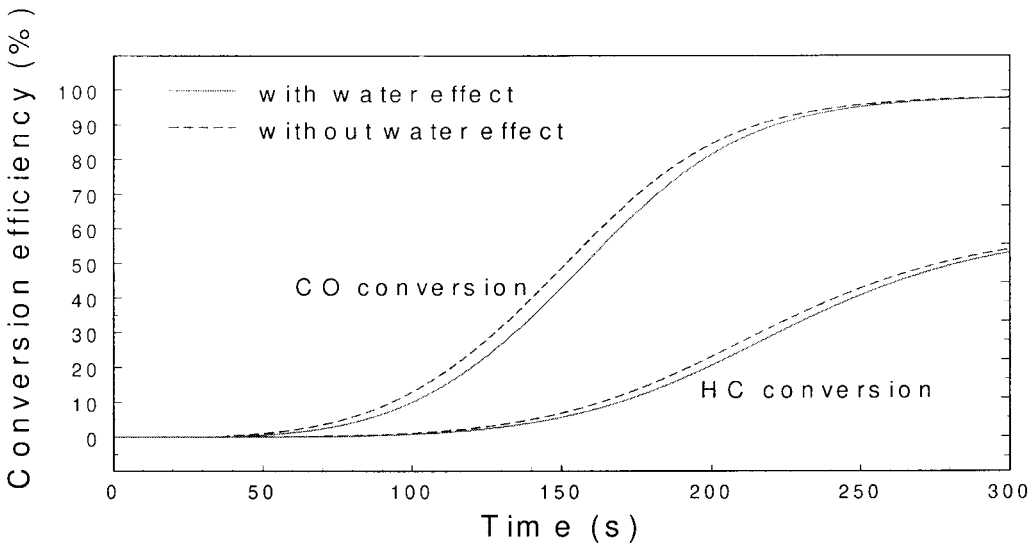

Fig. 18. Comparison of calculated conversion efficiencies of the catalyst in the cases of including and ignoring water condensation effect (Case 1)

15 (Case 1) shows that the predicted THC is slightly underestimated, whilst Fig. 16 (Case 2) shows predicted CO is slightly overestimated. In general, the predictive capability of the model is acceptable both in thermal and chemical aspects.

The effect of water condensation on surface heat transfer at engine cold-start included in the present model is the main cause of improved predictive capability of the model, which has not been achieved by others thus far. This effect is clearly shown by comparing the predicted results, with and without the inclusion of water condensation effect, with experimental data. Fig. 17 shows a comparison of gas temperatures predicted by the simulation model, with the water condensation ignored, with the experimental data in the case of idling engine speed of 2000 rpm. It is obvious that ignoring water condensation effect increases heat transfer from exhaust gas to the catalyst wall and causes the catalyst monolith to be heated up faster than that in actual situation. This means that the water condensation effect impedes the warming up process and causes prolonged lightoff time of catalysts at engine cold-start as illustrated in Fig. 18.

6. Conclusions

An exhaust system including a TWC was successfully modelled and tested under engine cold-start conditions. The authors would like to conclude that:

- Wet surface heat transfer at catalyst monolith is important during the engine warming up period, which affects the prediction of dew point temperature platform.
- The lightoff point of the catalytic converter reflected by the conversion of THC occurred at around 300°C, which is a temperature usually used as a guideline for catalyst lightoff.
- Validation of the predicted results with experimental data showed that the predictive capability of the model is acceptable, both qualitatively and quantitatively.

Appendix A

Engine specifications

Model	Ford MVH 418
Number of cylinders	4 in-line
Bore	80.6 mm
Stroke	88 mm
Swept volume	1796 cm^3
Firing order	1-3-4-2
Maximum speed	6000 rpm
Compression ratio	10:1
Maximum power	77 kW at 5500 rpm
Maximum torque	153 Nm at 4000 rpm

Appendix B

Catalytic converter specifications

Type	TWC
Shape and dimensions	Oval: 169.7 × 80.8 × 63.1 mm
Frontal area	118.69 cm^2
Volume	2 × 0.75 l
Cell density	400 cpsi (62 cpsc), square cell
Substrate	Cordierite
Substrate density	430 g/l
Wall thickness	0.152 mm
Wash coating	JM (product of Johnson Matthey Technology Centre)
Loading	2119 g/m^3
Catalytic surface area	15 m^2/g

References

[1] S.T. Gulati, L.F. Jones, M.J. Brady, R. Baker, B. Kessler, M. Zammit, B Snider, S. Rajadurai, Advanced three-way converter system for high temperature exhaust aftertreatment, SAE paper 970265, 1997.

[2] J.P. Day, Substrate effects on lightoff—part I: thermal Energy Requirements, SAE paper 962074, 1996.

[3] S.D. Burch, T.F. Porter, M.A. Keyser, M.J. Brady, K.F. Michaels, Reducing cold start emissions by catalytic converter thermal management, SAE paper 950409, 1995.

[4] P. Degobert, Automobiles and Pollution, Society of Automotive Engineers, Paris, 1995.

[5] J. Zhu, S.H. Chan, An approach for rapid catalyst lightoff by high values of ignition retard, J. Inst. Energy 69 (1996) 144–155.

[6] Z. Liu, A.L. Hoffmanner, J.F. Skowron, M.J. Miller, Exhaust transient temperature response, SAE paper 950617, 1995.

[7] P.A. Konstantinidis, G.C. Koltsakis, A.M. Stamatelos, Transient heat transfer modelling in automotive exhaust systems. in: Proc. Instn. Mech. Engrs. 211, Part C, 1997.

[8] T. Yasgashi, K. Yoshizake, T. Nagami, S. Sugiuram, T. Yoshimaga, K. Ohsawa, New technology for reducing the power consumption of electrically heated catalysts, SAE paper 940464, 1994.

[9] N. Baba, K. Ohsawa, S. Sugiura, Numerical approach for improving the conversion characteristics of exhaust catalysts under warming-up condition, SAE paper 962076, 1996.

[10] G.C. Koltsakis, P.A. Konstantinidis, A.M. Stamatelos, Development and application range of mathematical models for 3-way catalytic converters, Applied Catalysis B: Environmental 12 (1997) 161–191.

[11] J.G. Collier, Convective Boiling and Condensation, McGraw-Hill, New York, 1981.

[12] D.B. Spanding, N.H. Afgan, A numerical study of a interchanging vapour, droplet and film flows in a gasoline engine manifold, in: B.E. Milton, M. Behnia (Eds.), Heat and Mass Transfer in Gasoline and Diesel Engines, Hemisphere, New York, 1989.

[13] V. Gnielinski, Int. Chem. Eng. 16 (1976) 359.

[14] H. Hausen, Heat Transfer in Counter Flow, Parallel Flow and Cross Flow, McGraw-Hill, New York, 1983.

[15] W.R. Moore, R.J. Mondt, Predicted cold start emission reductions resulting from exhaust thermal energy conservation to quicken catalytic converter light-off, SAE paper 931087, 1993.

[16] S.W. Churchill, H.H.S. Chu, Correlating equations for laminar and turbulent free convection from a horizontal cylinder, Int. J. Heat Mass Transfer 18 (1975) 1049–1053.

[17] E.M. Sparrow, J.L. Gregg, The variable fluid-property problem in free convection, in: Recent Advances in Heat and Mass Transfer, McGraw-Hill, New York, 1961, pp. 353–371.

[18] S.T. Lee, R. Aris, On the effects of radiative heat transfer in monolith, Chemical Engineering Science 32 (1977) 827–837.

[19] H. Byrne, J. Norbury, Mathematical modelling of catalytic converters, Math. Engng. Ind. 4 (1) (1993) 27–48.

[20] J.C. Kuo, C.R. Morgan, H.C. Lassen, Mathematical modelling of CO and HC catalytic converter systems, SAE paper 710289, 1971.

[21] B.J. Cooper, L. Keck, NiO incorporation in three-way catalyst systems, SAE paper 800461, 1980.

[22] S. Sugiura, K. Ijuin, T. Yamada, T. Yaegashi, N. Baba, A Multi-dimensional numerical method for predicting warm-up characteristic of automobile catalytic converter systems, SAE paper 952413, 1995.

[23] S. Siemund, J.P. Leclerc, D. Schweich, M. Prigent, F. Castagna, Three-way monolithic converter: simulation versus experiments, Chemical Engineering Science 15 (1996) 3709–3720.

[24] S.E. Voltz, C.R. Morgan, D. Liederman, S.M. Jacob, Kinetic study of carbon monoxide and propylene oxidation on platinum catalysts, Ind. Eng. Chem. Prod. Res. Dev. 12 (4) (1973).

[25] S.H. Oh, J.C. Cavendish, Ind. Eng. Prod. Res. Dev. 21 (1982) 29–37.

[26] D. Cundari, M.A. Nuti, One-dimensional model for monolithic converter: numerical simulation and experimental verification of conversion and thermal responses for two-stroke engine, SAE paper 910688, 1991.

[27] R.B. Bird, W.E. Stewart, E.N. Lightfoot, Transport Phenomena, Wiley, New York, 1960.

[28] S.H. Chan, J. Zhu, Modelling of cold-start engine

exhaust heat transfer and catalysts lightoff, J. Inst. Energy 71 (1999).
[29] L.C. Thomas, Heat Transfer, Prentice-Hall, New Jersey, 1992.
[30] C. Woodford, Solving Linear and Non-linear Equations, Ellis Horwood, 1992.
[31] A.R. Mitchell, D.F. Griffiths, The Finite-Difference Method in Partial Differential Equations, Wiley, 1980.